




| | |
|-------------------------------|---|
| Publication Year | 2016 |
| Acceptance in OA @INAF | 2021-01-18T09:58:48Z |
| Title | Stochastic reacceleration of relativistic electrons by turbulent reconnection: a mechanism for cluster-scale radio emission ? |
| Authors | BRUNETTI, GIANFRANCO; A. Lazarian |
| DOI | 10.1093/mnras/stw496 |
| Handle | http://hdl.handle.net/20.500.12386/29810 |
| Journal | MONTHLY NOTICES OF THE ROYAL ASTRONOMICAL SOCIETY |
| Number | 458 |

Stochastic reacceleration of relativistic electrons by turbulent reconnection: a mechanism for cluster-scale radio emission?

G. Brunetti¹ and A. Lazarian²

¹INAF/Osservatorio di Radioastronomia, via Gobetti 101, I-40129 Bologna, Italy

²Department of Astronomy, University of Wisconsin at Madison, 5534 Sterling Hall, 475 North Charter Street, Madison, WI 53706, USA

Accepted 2016 February 26. Received 2016 February 26; in original form 2015 July 26

ABSTRACT

In this paper, we investigate a situation where relativistic particles are reaccelerated diffusing across regions of reconnection and magnetic dynamo in super-Alfvénic, incompressible large-scale turbulence. We present an exploratory study of this mechanism in the intracluster medium (ICM). In view of large-scale turbulence in the ICM, we adopt a reconnection scheme that is based on turbulent reconnection and magnetohydrodynamics (MHD) turbulence. In this case, particles are accelerated and decelerated in a systematic way in reconnecting and magnetic-dynamo regions, respectively, and on longer time-scales undergo a stochastic process diffusing across these sites (similar to second-order *Fermi*). Our study extends on larger scales numerical studies that focused on the acceleration in and around turbulent reconnecting regions. We suggest that this mechanism may play a role in the reacceleration of relativistic electrons in galaxy clusters providing a new physical scenario to explain the origin of cluster-scale diffuse radio emission. Indeed differently from current turbulent reacceleration models proposed for example for radio haloes, this mechanism is based on the effect of large-scale incompressible and super-Alfvénic turbulence. In this new model, turbulence governs the interaction between relativistic particles and magnetic field lines that diffuse, reconnect and are stretched in the turbulent ICM.

Key words: acceleration of particles – magnetic reconnection – radiation mechanisms: non-thermal – turbulence – galaxies: clusters: general.

1 INTRODUCTION

Magnetic reconnection is a long-standing problem in astrophysics and plasma physics. The traditional Sweet–Parker model of reconnection (Parker 1957; Sweet 1958) is very slow in all the astrophysical settings, which induced to searches of faster reconnection schemes. Petschek (1964) or X point reconnection for years has been the major contender for the mechanism for fast astrophysical reconnection. With plasma effects, e.g. Hall effect, included, the Petschek scheme looked promising to many researchers in the field (e.g. Shay et al. 1998; Birn et al. 2001; Bhattacharjee 2004).

In parallel, a scheme that invokes 3D Alfvénic turbulence was suggested in Lazarian & Vishniac (1999, hereafter LV99). The process appealed to magnetohydrodynamics (MHD) turbulence properties and predicted the independence of the reconnection rates on microphysics. Numerical simulations with externally induced turbulence supported analytical predictions in LV99 (e.g. Kowal, de Gouveia Dal Pino & Lazarian 2011, 2012).

More recently, the Petschek scheme evolved into tearing reconnection, which presents much more chaotic state of the magnetic field evolution (Loureiro, Schekochihin & Cowley 2007; Uzdensky, Loureiro & Schekochihin 2010). Numerical simulations of tearing reconnection show a transition to turbulent state, although the role of turbulence for the reconnection in these simulations is debated (see e.g. Karimabadi & Lazarian 2013 for review). Other simulations are suggestive of fast, i.e. independent of resistivity, magnetic reconnection even in the case when turbulence is not induced externally, but is generated by reconnection itself (Beresnyak 2013; Lazarian et al. 2015; Oishi et al. 2015).

These two schemes, the turbulent and tearing one, present at the moment two competing reconnection processes, which, as we discuss further in the paper, can be complementary and synergetic. In view of large-scale turbulence being present in the intracluster medium (ICM; see e.g. Brunetti & Jones 2014, hereafter BJ14; Brüggén & Vazza 2015 for reviews), within this paper we mostly focus on the turbulent magnetic reconnection scheme.

The main aim of this paper is to explore a scenario of particle acceleration in the ICM where relativistic electrons are reaccelerated by the combined effect of super-Alfvénic turbulence and magnetic

* E-mail: brunetti@ira.inaf.it

reconnection. As already mentioned, turbulence and magnetic reconnection are interconnected aspects and reconnection can be fast in the presence of turbulence (see LV99; Lazarian et al. 2015 for review). In the presence of super-Alfvénic turbulence, relativistic particles can diffuse across a complex network of regions of reconnection and magnetic field dynamo, where they are systematically accelerated or decelerated. This situation can be described as a combination of a first-order *Fermi* acceleration and a second-order *Fermi* acceleration due to spatial random-walk across accelerating and decelerating regions. Under the assumption of *fast* diffusion from reconnection regions, this chain of mechanisms becomes a second-order acceleration process and is the main focus of this paper.

Galaxy clusters are potential sites for this mechanism because super-Alfvénic turbulence is generated in the ICM. Evidence for relativistic electrons and magnetic fields in the ICM is routinely obtained from a variety of radio observations that detect diffuse synchrotron radiation from the ICM in the form of radio haloes and relics (see Ferretti et al. 2012; BJ14 for reviews). Giant radio haloes and relics are found in disturbed clusters, suggesting that large-scale motions that are generated during mergers provide the energy reservoir for the mechanisms of *in situ* particle acceleration (see BJ14 for review on acceleration mechanisms in the ICM).

A popular scenario for the origin of radio haloes is based on reacceleration induced by merger-driven turbulence (see Brunetti et al. 2001; Petrosian 2001; Fujita, Takizawa & Sarazin 2003; Brunetti et al. 2004; BJ14 for review). In this model, it is usually assumed that large-scale compressive turbulence generated during cluster mergers is transported at smaller scales via turbulent cascade and reaccelerates seed electrons (Cassano & Brunetti 2005; Brunetti & Lazarian 2007). This scenario has the potential to explain the observed properties of radio haloes and it naturally explains their connection with mergers, still several challenges exist. Primarily the challenge is to determine the efficiency of particle acceleration that depends on the complex hierarchy of mechanisms that transport energy from large-scale motions to collisionless particle-wave interactions at small scales in the ICM (see e.g. Brunetti 2016 for a recent discussion). An additional challenge is that turbulent acceleration in the ICM is a slow process that cannot accelerate particles directly from the thermal pool (e.g. Petrosian & East 2008). For this reason, turbulent acceleration models require a population of seed electrons that are already ultrarelativistic (e.g. $\gamma \geq 100$) and that are spatially distributed on cluster scales (e.g. Brunetti et al. 2001; Brunetti & Lazarian 2011a; Pinzke, Oh & Pfrommer 2015).

More recently, numerical (fluid) simulations suggested that the compressive part of turbulence in the ICM is partially dissipated into weak shocks (see Miniati 2015; Porter, Jones & Ryu 2015), implying that less energy is available for the mechanisms that are generally invoked in turbulent reacceleration models.

In order to overcome this last challenge, we exploit our mechanism that is based on incompressible turbulence. We show that this mechanism may play a role in the reacceleration of relativistic electrons in the ICM under reasonable assumptions on the effective particle mean free path (mfp).

In Section 2, we discuss turbulent reconnection in super-Alfvénic turbulence. In Section 3, we explain the acceleration mechanism and in Section 4 we apply it to the case of cluster-scale radio emission in galaxy clusters. In Section 5, we provide a discussion on cosmic rays (CRs) acceleration in the ICM and on the comparison between our model and other turbulent reacceleration models. We summarize results in Section 6.

2 TURBULENCE AND MAGNETIC RECONNECTION

The ICM is a *weakly collisional* high-beta plasma and is expected to be turbulent at some level (see BJ14; Brüggén & Vazza 2015 for reviews), the presence of instabilities in this plasma would make turbulence similar to MHD one (see Santos-Lima et al. 2014 and references therein). Natural drivers of ICM turbulence are the motions gravitationally driven by dark matter substructures that are generated in the ICM as a consequence of the hierarchical process of formation of galaxy clusters. As a consequence of these motions super-Alfvénic and subsonic turbulence should be driven in the ICM, although the way this turbulence is transported from large scale to small scale depends on details of ICM microphysics that are still poorly understood. It is believed that a hierarchy of processes in the ICM convert turbulent energy into non-linear amplification of magnetic fields, and particle heating and acceleration (e.g. Ryu et al. 2008; BJ14; Miniati & Beresnyak 2015).

Magnetic reconnection and dynamo are part of the turbulent cascade (e.g. Lalescu et al. 2015) and play a role in this complex hierarchy of mechanisms. Specifically, the model of turbulent reconnection by LV99 provides a natural extension of the classical Sweet–Parker model in the presence of turbulent motions.

Macroscopically, the reconnection speed is constrained by the possibility to eject the plasma from the reconnection layer. It gives a maximum reconnection speed on macroscopic scales:

$$V_{\text{rec}} \approx V_A \frac{\Delta}{l_X}, \quad (1)$$

where Δ is the thickness of the reconnection region (current sheet) and l_X is the astrophysical scale of the inflow associated with a reconnection region. In the classical Sweet–Parker model, two regions with uniform *laminar* magnetic fields are separated by a thin current sheet, which is determined by microscopic resistivity. Over the thickness of this thin current sheet, Δ , the resistivity is important and the magnetic fields reconnect. However in astrophysical situations, the disparity of scales between the inflow, l_X , and the outflow, Δ , strongly limit the reconnection rate (from equation 1), implying $V_{\text{rec}} \ll V_A$.

One possibility to overcome this bottleneck is turbulence. Turbulence changes the direction of magnetic field lines that are subject to turbulent diffusivity. Under these conditions, the outflow Δ gets much thicker, being determined not by microphysics of resistivity, but by macroscopic field wandering in 3D (LV99). LV99 derived the reconnection rate for sub-Alfvénic turbulence, this is $V_{\text{rec}} \sim (l_X/L_0)^{1/2} M_A^2 V_A$, where L_0 and M_A are the turbulent injection scale and Alfvén Mach number, respectively.

Results can be easily extended into the super-Alfvénic regime (Lazarian et al. 2015) that is typical of the ICM. An intuitive way to estimate Δ in super-Alfvénic turbulence is to use the diffusion properties of magnetic field lines. In this approach, Δ is essentially the diffusion scale covered by magnetic field lines within the time-period necessary to expel the plasma from the reconnection region, $\tau_A \sim l_X/V_A$. It has been shown that field diffusion in these conditions is similar to Richardson diffusion in hydromotions (Eyink et al. 2013). It implies $\Delta^2 \approx \epsilon \tau_A^3$, where $\epsilon \sim \delta V^3/L_0$ is the specific turbulent energy rate, from which one immediately gets $\Delta \sim l_A$.

The other ingredient to determine a macroscopic constraint to the reconnection speed in equation (1) is the inflow, astrophysical, scale of reconnection regions l_X . Super-Alfvénic turbulence naturally generates regions of magnetic field reversals everywhere in the plasma with minimum scale of the order of the MHD scale

$l_A = L_o M_A^{-3}$. At scales $l > l_A$, kinetic energy is in excess of magnetic energy inducing a continuous change of magnetic field topology, due to advection of field lines by hydromotions, and consequently quenching the reconnection process. Under these conditions, the dominant scale for the inflow in reconnection regions is expected to be $l_X \sim l_A$.

As a consequence, we may think of a situation of *fat* reconnection regions in super-Alfvénic turbulence, with $\Delta \sim l_X \sim l_A$, where the macroscopic reconnection speed can approach the Alfvén speed (equation 1).

In the following, we shall adopt this configuration to calculate particle acceleration.

3 ACCELERATION OF RELATIVISTIC PARTICLES IN RECONNECTION

3.1 Brief overview on acceleration in turbulent reconnection

Particle acceleration in reconnection regions has been investigated in different environments and considering different mechanisms (e.g. Lyubarsky 2003; Lyutikov & Blandford 2003; Drake et al. 2006, 2010; Lazarian & Opher 2009; Lazarian & Desiati 2010; Kowal et al. 2011; Drake, Swisdak & Fermo 2013; Giannios 2013; Sironi & Spitkovsky 2014; Zank et al. 2014).

One mechanism has been proposed within turbulent reconnecting regions. Turbulent reconnection results in shrinking of 3D magnetic bundles and the charged particles entrained over magnetic loops can be accelerated by first-order *Fermi* mechanism (de Gouveia dal Pino & Lazarian 2005). This mechanism has been used to model particle acceleration in several environments, including γ -ray bursts (Zhang & Yan 2011), low-luminosity AGNs (Kadowaki, de Gouveia Dal Pino & Singh 2015), microquasars (Khiali, de Gouveia Dal Pino & del Valle 2015) and in the heliosphere (Lazarian & Desiati 2010). Interestingly, the compressibility is not necessary in this mechanism.¹ The physics of the acceleration is easy to understand. Magnetic reconnection induces systematic shrinking of magnetic field lines on scales $\leq l_A$ and particles entrained on these field lines are getting energy as the consequence of the Liouville theorem.

Particle acceleration in turbulent reconnection sites has also been investigated by numerical studies that combine MHD simulations and tracer particles (e.g. Kowal et al. 2011, 2012). The acceleration of particles trapped within converging reconnection regions is consistent with first-order *Fermi* mechanisms.

In a general situation presumably particles interact with multiple reconnection layers and turbulence experiencing a hierarchy of processes at different scales and energies. An exploratory investigation of this situation is the main focus of this section (Section 3.2). However, we anticipate that the basic picture deriving from our study does not depend critically on the specific mechanism of particle acceleration within reconnecting regions (see Section 3.3).

3.2 Our approach

Here, we follow a simple approach to explore the general situation where relativistic particles are reaccelerated diffusing on large-scale

super-Alfvénic turbulence and reconnection regions. We proceed with the following assumptions:

- (i) large-scale turbulence in the ICM behaves collisional and MHD provides a good guide as far as reconnection is considered;
- (ii) ultrarelativistic CRs are collisionless components interacting with fluctuations in the MHD fluid;
- (iii) we assume a scenario based on turbulent reconnection, where diffusion of magnetic field lines governs the process of scattering of CRs;
- (iv) we expressly investigate only the collisionless effects that involve the interactions between large-scale magnetic field lines and CRs.

It is difficult to establish to what extent these assumptions allow a solid description of the ICM. The main point here is that we need reconnection events in terms of (belonging to) MHD cascade. However, it is worth to note that even if turbulence in the ICM is collisionless we may still expect that the dynamics of the magnetic field lines can be described according to Alfvénic turbulence (Eyink, Lazarian & Vishniac 2011; Makwana et al. 2015), thus supporting our basic assumptions.

We start considering particles within reconnecting regions. The increment in momentum of particles after the interaction with shrinking magnetic field lines can be estimated as

$$\Delta p \simeq \Delta t \times \frac{dp}{dt}, \quad (2)$$

where the time-scale spent by particles in a reconnecting region is

$$\Delta t = \min \left\{ \frac{l_A}{V_A}, \frac{l_A^2}{D} \right\}, \quad (3)$$

where $\frac{l_A}{V_A}$ is the turn-over time of eddies (corresponding to *slow* diffusion limit) and $\frac{l_A^2}{D}$ is the particle diffusion time on scale l_A (corresponding to *fast* diffusion, D is the spatial diffusion coefficient of CRs), and

$$\frac{dp}{dt} \sim \phi \frac{V_A}{\lambda_{\text{mfp}}} p, \quad (4)$$

where λ_{mfp} is the particles mfp and $\phi \sim 1$ accounts for pitch angle distribution and geometry of scatterings.

However, in a turbulent fluid with stationary turbulence the reconnection process should be accompanied by the opposite process of magnetic field generation, i.e. by turbulent dynamo. Naturally, this process results in a stretching and expansion of the magnetic field lines that on scale l_A occurs on a time-scale l_A/V_A and that *statistically* compensates field diffusion on the same scale (Beresnyak & Lazarian 2015). It results in a situation where energetic particles within dynamo regions cool by an amount that is similar (in absolute value) to that of the acceleration in reconnection regions.

Therefore if particles can diffuse across these regions, we expect that they will undergo cycles of first-order acceleration in reconnection regions and cycles of cooling in dynamo regions. This is the theoretical picture that we use to describe the acceleration of particles diffusing in a turbulent fluid on scales larger than l_A . It differs from the traditional second-order *Fermi* acceleration because the increments of the momentum of the CR in the acceleration and deceleration regions in principle can be comparable with the momentum of the CR.

In order to estimate the acceleration rate resulting from this complex mechanism, we make the educated guess that reconnecting and dynamo regions are statistically distributed everywhere in the

¹ A generalized version of the mechanism in the presence of compression is discussed in Drury (2012).

astrophysical volume on typical scales $\sim l_A$. This can be motivated by the fact that the generation of magnetic fields and field reconnection occur indeed everywhere in the volume, although this assumption needs to be evaluated more carefully in follow up studies.

For $\Delta p \ll p$ in equation (2), particles interacting with these regions will undergo a random-walk process in the momentum space resembling a second-order *Fermi* mechanism. From equations (2)–(4) this condition implies $\lambda_{\text{mfp}} \gg \phi l_A$ (in the slow diffusion) or $\lambda_{\text{mfp}} > l_A (3\phi V_A/c)^{1/2}$ (*fast* diffusion, assuming $D \sim \frac{1}{3}c\lambda_{\text{mfp}}$). This also tells us that the condition $\Delta p \ll p$ in the ICM is possible only in the case of *fast* diffusion, because *slow* diffusion (equation 3) occurs for $\lambda_{\text{mfp}} \leq 3V_A l_A/c \ll l_A$.

In the following, we will restrict to the case of fast diffusion and to situations where $\Delta p \ll p$. Under these conditions, particles undergo a diffusion process in the momentum space and retain an isotropic distribution of pitch angles, provided that the pitch-angle scattering rate, $\tau_{\text{sc}} \sim \lambda_{\text{mfp}}/c$, is fast enough. The distribution function of particles in the momentum space, $f(p)$, evolves according to a isotropic Fokker–Planck equation (e.g. Schlickeiser 2002):

$$\frac{\partial f(p, t)}{\partial t} = \frac{1}{p^2} \frac{\partial}{\partial p} \left(p^2 D_{\text{pp}} \frac{\partial f}{\partial p} - p^2 \sum \left| \frac{dp}{dt} \right|_{\text{loss}} f(p, t) \right) + Q(p, t) - \frac{f(p, t)}{T_{\text{esc}}}, \quad (5)$$

where the diffusion coefficient in the particle momentum space is (equations 2–4)

$$D_{\text{pp}} = \left\langle \frac{\Delta p \Delta p}{2\Delta t} \right\rangle \sim 3 \left(\frac{l_A}{\lambda_{\text{mfp}}} \right)^2 \frac{V_A^2}{\lambda_{\text{mfp}} c} p^2 \quad (6)$$

implying a reacceleration time $\tau_{\text{acc}} \sim p^2/(4D_{\text{pp}})$, and where $\sum \left| \frac{dp}{dt} \right|_{\text{loss}}$ accounts for the energy losses in the ICM (synchrotron, ICS, Coulomb,...), Q accounts for injection of new particles, and f/T_{esc} accounts for diffusion/escape of particles from the region (T_{esc} is the escaping time).

Solutions of equation (5) in the case $D_{\text{pp}} \propto p^2$ are calculated in numerous papers (see e.g. Schlickeiser 1984; Mertsch 2011, for numerical solutions Donnert & Brunetti 2014, and references therein). We anticipated that $D_{\text{pp}} \propto p^2$ also results from reacceleration by compressible turbulence (both transit-time damping – TTD – and stochastic compressions) in the ICM and consequently the properties of the spectra of reaccelerated electrons expected in our model will be similar to those calculated in other studies (BL07; Brunetti & Lazarian 2011a; ZuHone et al. 2013; Donnert & Brunetti 2014; see sections 4 and 5).

The acceleration rate from equation (6) depends on the particles mfp that however is poorly known. In super-Alfvénic turbulence hydromotions change directions of magnetic field lines on scales $\geq l_A$. This configuration automatically defines a maximum effective mfp of particles, $\lambda_{\text{mfp}} \sim l_A$, because particles travelling in tangled fields change directions on this scale preserving the adiabatic invariant. In addition magnetic field fluctuations in MHD turbulence induce particles pitch-angle scattering via resonant interaction and affect the motion of particles. This is different from the previous interaction because in this case particles experience pitch-angle scattering with respect to the local field direction and do not

preserve adiabatic invariant. The parallel mfp from this process is

$$\lambda_{\text{mfp}} = \frac{3c}{4} \int_0^1 d\mu \frac{(1-\mu^2)^2}{D_{\mu\mu}}, \quad (7)$$

where $D_{\mu\mu}$ is the pitch-angle diffusion coefficient. In the case of incompressible MHD turbulence on scales $< l_A$ resonant pitch-angle scattering is dominated by TTD with pseudo-Alfvén modes (Yan & Lazarian 2008; Beresnyak, Yan & Lazarian 2011). In the super-Alfvénic case, the interaction is dominated by the largest moving mirrors with $l \sim l_A$, and from equations (8–9) in Yan & Lazarian (2008, in the limit $M_A \rightarrow 1$ and $L \rightarrow l_A$) we find $D_{\mu\mu} \sim \frac{c}{l_A} F(\mu)$, where $F(\mu) \sim 1$ for transverse propagation and $F \ll 1$ in the quasi-parallel case. In this case, equation (7) gives $\lambda_{\text{mfp}} \sim l_A$.

In conclusion, particles interacting with large-scale incompressible and super-Alfvénic MHD turbulence will change direction on time-scales $\sim l_A/c$ due to magnetic field tangling and at the same time will experience pitch-angle scattering on time-scale $\sim F(\mu)^{-1} l_A/c$. It basically implies an average effective mfp that is a fraction of l_A , $\lambda_{\text{mfp}} = \psi l_A$, where $\psi < 1$; additional mechanisms of pitch-angle scattering from kinetic/plasma effects will further reduce λ_{mfp} (Section 3.3).

It is thus convenient to re-write relevant quantities in terms of $\beta_{\text{pl}} = 2\Gamma^{-1} c_s^2/V_A^2$ ($\Gamma = 5/3$) and the particles mfp in terms of the Alfvén scale, l_A :

$$D_{\text{pp}} \simeq 3\sqrt{\frac{5}{6}} \frac{c_s^2}{c} \frac{\sqrt{\beta_{\text{pl}}}}{L_o} M_t^3 \psi^{-3} p^2 \quad (8)$$

and

$$l_A = L_o M_A^{-3} = \frac{(6/5)^{3/2} L_o}{(\sqrt{\beta_{\text{pl}}} M_t)^3}. \quad (9)$$

Note that the condition $\Delta p \ll p$ is satisfied for

$$\psi > \sqrt{\frac{(3c_s \sqrt{6/5})}{(c \sqrt{\beta_{\text{pl}}})}}. \quad (10)$$

3.3 A note on the role of kinetic effects

The role of kinetic effects on small scales is different for the turbulent reconnection (see LV99; Kowal et al. 2009; Eyink et al. 2011, 2013; Eyink 2015; Lazarian et al. 2015) and tearing reconnection (see Loureiro et al. 2007; Uzdensky et al. 2010; Ng et al. 2015). Kinetic effects in the latter process accelerate the reconnection rate inducing tearing of the current sheet. On the contrary, turbulent reconnection is independent of the detailed kinetic physics, as follows from theory (LV99; Eyink 2015) and confirmed in numerical simulations where plasma physics effects were introduced using anomalous resistivity (see Kowal et al. 2009). Both approaches can be complementary with tearing destabilizing the reconnection sheet if the level of turbulence in the system is low. The outflow from the reconnection layer for extended current sheets has the thickness Δ and the *Reynolds* number $Re \sim V_A \Delta/\nu$, where ν is viscosity, which for the ICM should be taken the perpendicular Braginsky viscosity. With tearing inducing $V_{\text{rec}} > 0.01 V_A$, which in turn is of the order of $V_A \Delta/l_x$ (equation 1), Δ gets to be $> 0.01 l_x$, making the *Reynolds* numbers of the outflow sufficiently large. This should make the outflow turbulent and is likely to transfer the reconnection into a regime similar to turbulent reconnection.

The physics of acceleration in turbulent and tearing reconnection in 3D is very similar. The difference initially were due to the fact

that acceleration in turbulent reconnection was considered in 3D (de Gouveia dal Pino & Lazarian 2005) while acceleration in tearing was considered in 2D (Drake et al. 2006). As the actual 3D geometry of astrophysical reconnection is being acknowledged and tearing reconnection layers demonstrate more turbulence as the numerical resolution increases, strong similarities emerge between the two mechanisms with the acceleration being essentially related to the shrinking of 3D loops.²

It is also true that particle acceleration and transport in reconnection regions are potentially sensitive to details of the physics of reconnection (e.g. Daughton et al. 2011). More recently the controversy on whether the tearing reconnection is second or first order has emerged. For example, Drake et al. (2013) find a shortening of magnetic island field line length because of adjacent islands merging. This causes an increase in the parallel particle velocity and a decrease in perpendicular energy suggesting second order rather than first-order *Fermi* mechanisms. In fact, attempts to model second-order *Fermi* acceleration of particles diffusing across multiple reconnecting regions have been developed in the case of collisionless tearing reconnection mediated by quasi-2D magnetic islands (e.g. Le Roux et al. 2015).

In Section 3.2, we have assumed first-order acceleration in reconnection regions because this mechanism has been clearly demonstrated in numerical simulations of turbulent reconnection (Kowal et al. 2012). We would believe that a similar effect should be present also in tearing reconnection. While the relative importance of the second- and first-order *Fermi* acceleration in tearing reconnection may need to be settled in future, for our treatment of the acceleration this is not so vital and in principle our picture can be extended also to the case of tearing reconnection. In fact, we only require that a particle leaving the reconnection region gained the momentum Δp whatever is the cause of the acceleration.³ Once CRe leave reconnecting regions they will interact with the dynamics of magnetic field lines on very large scales, $l_A \sim 100$ pc – kpc. On these large scales reconnection events are part of the turbulent cascade and we can use transport properties that follow from MHD turbulence (Section 3.2).

The microphysics of the plasma may still be important for particle acceleration and reacceleration even if the reconnection rates are determined by the LV99 mechanism. In fact, kinetic/plasma effects on small scales may induce pitch-angle scattering events in addition to those due to the MHD fluctuations on large scales considered in Section 3.2. Overall, the combined effects of scatterings on small and large scales can be parametrized in the form of the particles mfp, λ_{mfp} , and in general scatterings on small scales are expected to reduce λ_{mfp} with respect to that in Section 3.2 and increase the acceleration rate. We note that the small-scale physics is likely to be important when we consider the acceleration of particles from the thermal pool. In this respect, potentially kinetic/plasma effects might provide also a solution to the problem of *seed* particles in reacceleration models (Section 1), however we do not address the issue of the acceleration of energetic particles from the thermal pool in this paper.

² A comparison of particle acceleration rates in 2D and 3D configurations is discussed in Kowal et al. (2011).

³ In the case of second-order acceleration, the term dp/dt in our equation (4) can be seen as the *systematic* part of a second-order process occurring within reconnection regions, i.e. $dp/dt \sim \bar{D}_{pp}/4p$ where \bar{D}_{pp} is the diffusion coefficient in the particles' momentum space due to such a hypothetical second-order mechanism on smaller scales.

4 DIFFUSE RADIO EMISSION IN GALAXY CLUSTERS

4.1 Current view

Turbulence and shocks are generally invoked to play a role for the origin of radio haloes and radio relics in galaxy clusters (BJ14 for review). Nevertheless recent observations of the radio relic in A2256 unveiled a complex/filamentary morphology of the radio emission and no clear evidence for a direct connection with a shock, hinting a possible role of magnetic reconnection (Owen et al. 2014). A role of magnetic reconnection for the origin of non-thermal components in galaxy clusters was also envisaged on theoretical grounds by Lazarian & Brunetti (2011).

Radio haloes are the most prominent non-thermal sources in galaxy clusters. A popular scenario for their origin is based on the hypothesis that turbulence generated during cluster mergers (re)accelerates seeds electrons on Mpc scales (Brunetti et al. 2001; Petrosian 2001, BJ14 for review). Crucial ingredients of this scenario are however poorly known. Primarily the challenge is to understand the chain of mechanisms that allow us to drain energy from large-scale motions into mechanisms acting on smaller scales and that in turn determines the efficiency of acceleration (see Brunetti 2016 for a recent discussion).

Presumably several turbulent components are generated in the ICM, both at large and very small scales, and all these components should jointly contribute to the scattering and (re)acceleration of relativistic particles. In the last years, much attention has been devoted to the role of compressible turbulence that is driven at large scales in the ICM from cluster mergers and that cascades at smaller scales (Cassano & Brunetti 2005; Brunetti & Lazarian 2007, 2011a). This is the simplest scenario that can be thought, nevertheless it predicts a straightforward connection between cluster mergers and radio haloes in agreement with observations. This is also the scenario adopted in follow-up numerical simulations that aim at investigating the origin of diffuse radio emission in galaxy clusters (Beresnyak et al. 2013; Donnert et al. 2013; Donnert & Brunetti 2014; Miniati 2015; Pinzke et al. 2015).

On the other hand, recent numerical simulations of cluster formation have shown that most of the turbulence in galaxy clusters is solenoidal (see Miniati 2015). Although these simulations show that compressive turbulence is also generated in connection with clusters mergers, this component is found fairly short living (\leq Gyr) and with a kinetic spectrum that is steeper than that previously assumed in calculations of turbulent acceleration. The consequence is a reduction of both the reacceleration period and the acceleration rate. In reality, these simulations do not tell us much about the microphysics (e.g. particles collision frequency) and power spectrum of electromagnetic fluctuations that both govern the acceleration efficiency and *di per se* do not challenge acceleration models based on compressive turbulence generated at large scale (Miniati 2015; Brunetti 2016). However, these are clearly thought-provoking results that motivate us to investigate possible mechanisms that drain a fraction of the solenoidal turbulence in the ICM into particle acceleration.

4.2 A new mechanism?

In this respect, the mechanism described in Section 3 is particularly attractive as it is based on super-Alfvénic solenoidal turbulence. If

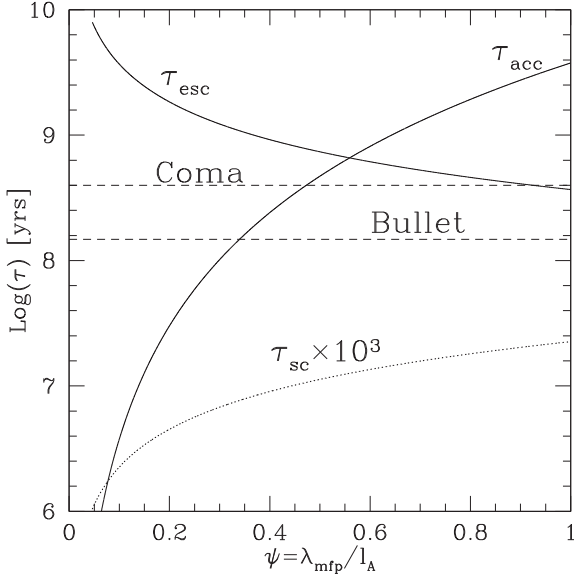


Figure 1. Acceleration time-scales as a function of ψ . Horizontal dashed lines are the maximum reacceleration times, τ_{\max} , required for the radio haloes in the Coma and Bullet clusters (equation 14, see the text). Diffusion time on $L_{\text{RH}} = 1$ Mpc (equation 12) and scattering time-scale, λ_{mfp}/c (multiplied by 1000 for display proposal), are also reported. Calculations are obtained assuming $M_t^2 = 0.25$, $L_o = 300$ kpc, $\beta_{\text{pl}} = 60$, $c_s = 1500$ km s $^{-1}$.

we restrict to the situation of *fast* diffusion regime, the acceleration time is (equation 8)

$$\tau_{\text{acc}} = \frac{p^2}{4D_{\text{pp}}} \simeq \frac{\sqrt{6/5}}{12} \frac{c}{c_s^2} \frac{L_o}{\sqrt{\beta_{\text{pl}}}} M_t^{-3} \psi^3, \quad (11)$$

and the acceleration rate (or efficiency, throughout this paper) = τ_{acc}^{-1} . The acceleration time is reported in Fig. 1 as a function of the CRE mfp, $\psi = \lambda_{\text{mfp}}/l_A$, assuming typical conditions in the ICM; the acceleration efficiency rapidly increases with decreasing CRE mfp. Fig. 2 shows the effect induced on the acceleration time by increasing the turbulent Mach number and β_{pl} : for given values of ψ and of the turbulent injection scale, L_o , the acceleration rate increases with both Mach number and β_{pl} . Calculations in Fig. 2 are obtained for typical conditions in the ICM, specifically we assume a range of $\beta_{\text{pl}} \sim 30$ –120 that is inferred using values of magnetic field derived from Faraday rotation measures (e.g. Carilli & Taylor 2002; Feretti et al. 2012) and turbulent injection scales $L_o \geq 100$ kpc (BJ14; Brüggén & Vazza 2015).

In our model, the mfp is a free parameter that is difficult to calculate from first principles due to our ignorance of kinetic effects on small scales (see Section 3 for constraints based on MHD and 3.3 for a discussion on kinetic effects). However, we can also infer independent constraints on that. Statistics of radio haloes suggests that they are generated in massive mergers for a significant fraction of the duration of these events (e.g. Brunetti et al. 2009; Cassano et al. 2013; Cuciti et al. 2015). It implies that CRE should be trapped within the emitting, Mpc-scale, volume for \geq few Gyr. This provides a limit to the diffusion time of CRE on these scales and thus on their maximum mfp. The time needed by CRE to diffuse on the scale of a radio halo, L_{RH} , is

$$\tau_{\text{esc}} \sim \frac{L_{\text{RH}}^2}{4D} \sim \frac{5}{8} \sqrt{\frac{1}{6}} \frac{1}{c} \left(\sqrt{\beta_{\text{pl}}} M_t \right)^3 \frac{L_{\text{RH}}^2}{L_o} \psi^{-1} \quad (12)$$

that is reported in Fig. 1. The minimal condition $\tau_{\text{esc}} \geq$ few Gyr implies $\lambda_{\text{mfp}} \ll$ kpc, or in terms of MHD scale, $\psi < 0.5$

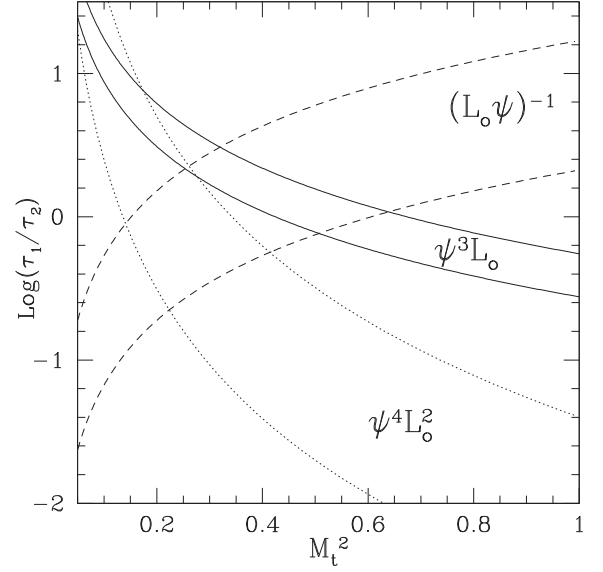


Figure 2. Ratio of model acceleration time and the $\tau_{\max} = 150$ Myr for the Bullet radio halo (solid lines), and ratio of model acceleration time and diffusion time on 1 Mpc (dotted lines) as a function of the turbulent Mach number. Calculations assume a reference value $\psi = 0.5$, and $\beta_{\text{pl}} = 30$ and 120 (from top to bottom); other parameters being equal to Fig. 1. Dashed lines are the diffusion times in Gyr (from top to bottom with decreasing β_{pl}). Dependences on ψ and L_o are shown in the panels.

$(\beta_{\text{pl}}/60)^{3/2} (M_t/0.5)^3 (L_o/300 \text{ kpc})^{-1}$ (Fig. 1, equation 12), i.e. larger values of the turbulent Mach number and of the β_{pl} constrain larger values of ψ . We note that the ratio of acceleration and diffusion time, $\tau_{\text{acc}}/\tau_{\text{esc}} \propto \psi^4 L_o^2 M_t^{-6}$, rapidly decreases with increasing the turbulent Mach number for a given value of ψ and of the injection scale L_o (Fig. 2).

Finally, we note that very small values of the mfp, that imply faster acceleration (equation 11), are also ruled out from the condition $\Delta p \ll p$ (equation 10).

Given these constraints on λ_{mfp} and ψ , the following point is to understand whether our mechanism can explain the diffuse radio emission observed in galaxy clusters. To fully address this point Fokker–Planck time-dependent calculations are necessary (equation 5). However, as we anticipated in Section 3.2, numerous papers carry out Fokker–Planck calculations of particle reacceleration in galaxy clusters in the case $D_{\text{pp}} \propto p^2$. These results can be automatically extended to our model and for this reason in this exploratory paper we do not focus on Fokker–Planck analysis.

In practice two main processes oppose to the reacceleration of CRE.

Synchrotron and inverse Compton losses balance the acceleration of CRE channelling an increasing fraction of the energy gained by CRE into radiation. The time-scale of radiative losses (radiative lifetime) of CRE is

$$\tau_{\text{rad}}(\gamma) = \gamma / \frac{d\gamma}{dt} = \frac{6\pi m_e c}{\sigma_T} \frac{\gamma^{-1}}{B^2 + B_{\text{cmb}}^2}, \quad (13)$$

where $B_{\text{cmb}} \simeq 3.25(1+z)^2 \mu\text{G}$ is the equivalent field due to inverse Compton scattering with photons of the cosmic microwave background. In the ICM, the CRE that produce synchrotron radiation in the radio band have energies \sim few GeV and radiative lifetimes $\tau_{\text{rad}} \sim 100$ Myr (see BJ14 for review). The acceleration mechanisms that generate steep spectrum radio emission in galaxy clusters should have an efficiency that is comparable to that of the radiative losses

of the CRe that emit the observed radio emission. Consequently, due to the balance between acceleration and losses, after a reacceleration period of about 100 Myr the spectrum of radio emitting CRe evolves slowly with time and approaches quasi-stationary conditions, provided that the acceleration rate is constant (see BJ14 for review and references therein).

The second process that opposes to reacceleration is more subtle and is due to physical mechanisms that may damp the turbulent spectrum reducing with time the energy flux that becomes available for the reacceleration of CRs. In this respect, the most obvious process is the damping (via collisionless dampings) of turbulence due to the same CRs that are reaccelerated. This mechanism may affect (reduce) the acceleration rate on longer time-scales (see BJ14 for review and references therein).

In this section, we consider only the first damping mechanism, due to radiative losses of CRe, whereas in Section 5.2 we will discuss the turbulence damping.

In practice, the most relevant point here is to check whether our mechanism allows reacceleration of CRe to the energies that are necessary to produce the synchrotron radiation observed in galaxy clusters. In Figs 1 and 2, the acceleration time is compared with the acceleration time that is required for radio haloes. This is not necessarily equivalent to the radiative cooling time of the CRe emitting at the observed radio frequencies, because radio haloes have very steep synchrotron spectra, $\alpha \sim 1-2$ (flux $\propto \nu^{-\alpha}$). In this respect, we use results from Cassano et al. (2010) that calculated synchrotron spectra in homogeneous models of compressive turbulent reacceleration (with $D_{pp} \propto p^2$) assuming reacceleration periods in the range $\Delta t/\tau_{acc} \sim 2-4$. They found that the spectra become steeper than those of typical radio haloes at frequencies greater than $\nu_s \sim \xi \nu_b$, where $\xi \sim 6-8$, and ν_b is the critical synchrotron frequency emitted by electrons having acceleration time equal to the time-scale of radiative losses, i.e. CRe with Lorentz factor $\gamma_b = \frac{6\pi m_e c}{\sigma_T} \tau_{acc}^{-1} / (B^2 + B_{cmb}^2)$. The highest frequency is generated in a magnetic field $B \sim B_{cmb}/\sqrt{3}$, since this is the field where CRe emitting at a given frequency have maximum lifetime. It leads to a *minimal* request for a mechanism being sufficient to reaccelerate CRe emitting at the observed frequency $\nu_o = \nu_s/(1+z)$. This condition corresponds to a *maximum* reacceleration time, τ_{max} :

$$\tau_{acc} \leq \tau_{max} = 156 \left(\frac{\xi}{\nu_o(\text{GHz})} \right)^{1/2} (1+z)^{-7/2} \quad (\text{Myr}). \quad (14)$$

In Figs 1 and 2, we report relevant values of τ_{max} derived from equation (14). These values are derived for the radio haloes in the Coma and Bullet clusters, $\tau_{max} = 400$ and $=150$ Myr, respectively, by considering observed steepening frequencies $\nu_o \simeq 1$ GHz for Coma (see e.g. Brunetti et al. 2013 and references therein) and $\simeq 5$ GHz for the Bullet cluster (a hint of steepening is observed in this cluster at ~ 8 GHz; Liang et al. 2000; Shimwell et al. 2014; Marchegiani & Colafrancesco 2015).

The comparison between τ_{max} and the reacceleration time predicted by our model selects the parameters space (M_t , ψ , L_o) that allows us to explain radio haloes. Specifically, the acceleration time predicted by our model (equation 11) leads to a steepening frequency:

$$\nu_s(\text{GHz}) \simeq 2.45 \left(\frac{c_s}{10^3 \text{km s}^{-1}} \right)^4 \frac{\beta_{pl} \xi}{10^2 7} \left(\frac{10^2 \text{kpc}}{L_o} \right)^2 \left(\frac{M_t 0.5}{0.5 \psi} \right)^6 \times \left(\frac{B_{\mu G}}{B_{\mu G}^2 + B_{cmb}^2} \right)^2 / 0.01 \quad (15)$$

implying that an emitting synchrotron frequency 10 times larger is produced by increasing the turbulent Mach number (or reducing the CRe mfp) by about 50 per cent, or by assuming a turbulent-injection scale that is three times smaller. For $B \simeq B_{cmb}/\sqrt{3}$, the Mach number and the observed steepening frequency in our model are connected via (from equation 15):

$$M_t \simeq 0.8 \frac{10^3 \text{km s}^{-1}}{c_s} \left(\frac{\nu_o(\text{GHz}) 7}{35 \xi} \right)^{1/6} \times \left(\frac{L_o}{10^2 \text{kpc}} \right)^{1/3} \frac{(1+z)^{11/6} \frac{\psi}{0.5}}{\left(\frac{n_{\text{ICM}}}{10^{-3}} \right)^{1/6}} \quad (16)$$

that allows us to conclude that turbulent Mach numbers $M_t^2 \sim 0.2-0.5(\psi/0.5)^2(L_o/300 \text{kpc})^{2/3}$ are sufficient to reaccelerate CRe that generate synchrotron radio emission in hot, kT $\sim 5-15$ keV, clusters. Note that under these conditions, the model satisfies also the additional requirements that are necessary to explain radio haloes and cluster-scale radio emission, specifically the acceleration time is shorter than the diffusion time of CRe ($\tau_{acc} < \tau_{esc}$) and CRe are efficiently trapped within Mpc-scale emitting regions, i.e. $\tau_{esc} > \text{few Gyr}$ (Figs 1 and 2). We note that the above amount of turbulent energy/Mach numbers is consistent with that found in high-resolution cosmological (fluid) simulations (e.g. Vazza et al. 2011; Miniati 2015).

Interestingly, the same turbulent motions that are used in our model to reaccelerate particles will induce a broadening of the X-ray lines (for example the Fe xxv lines at 6.7 keV) that can be tested by the forthcoming ASTRO-H satellite (Kitayama et al. 2014) and, in the not too distant future, by ATHENA (Ettori et al. 2013). In particular, assuming a typical electron number density $= 10^{-3} \text{cm}^{-3}$, from equation (16) we get *minimum* turbulent velocities at the scale L_o , $\delta V_o \sim 780$ and $450 (\psi/0.5)(L_o/100 \text{kpc})^{1/3} \text{km s}^{-1}$ for the halo in the Bullet and Coma clusters, respectively (corresponding to Mach numbers $\simeq 0.39$ and 0.3 , respectively, see also Section 5).

At this point, it is worth to comment that our conclusions are based on results from compressive turbulent acceleration models in the homogeneous case and on their scaling to our model. Follow up Fokker-Planck time-dependent calculations combined with numerical simulations are required to account for non-homogeneous distributions of the physical parameters in the turbulent ICM (see discussion in Section 4.3) and to model the time evolution of the synchrotron spectrum of cluster-scale emission. For example, with regard to this latter point, the parameter $\xi \sim 6-8$ in equations (14)–(16) is derived for acceleration periods $\Delta t/\tau_{acc} \sim 2-4$ (Cassano et al. 2010, i.e. $\Delta t \sim 0.3-1$ Gyr for typical values of τ_{acc}), corresponding to a situation where radio spectra evolve slowly with time (quasi-stationary) because reacceleration is balanced by the energy losses of the CRe emitting in the radio band. On the other hand, the shape of the spectrum of radio haloes may be different during earlier and/or later phases. During earlier phases, reacceleration is not balanced yet by losses and the spectrum rapidly evolves with time being very steep (implying smaller ξ) at the beginning of the reacceleration phase ($\Delta t/\tau_{acc} < 2$). Similarly, at later stages the evolution of CRe spectrum is potentially affected by saturation effects due to turbulence damping (see Section 5).

4.3 A note on the spectrum of radio haloes

The spectral shape of radio haloes provides information that go beyond simple arguments based on acceleration time-scales. Unfortunately due to observational limitations, a spectrum with at least three measurements is available only for a few haloes, and

significant scatter of measurements is seen in the cases where the data points cover at least one order of magnitude in frequency range (e.g. Macario et al. 2013; Shimwell et al. 2014). Current studies suggest that the spectra of radio haloes are quite different. Assuming a simple power-law shape (in the form flux $\propto \nu^{-\alpha}$), the spectral slopes measured between two typical frequencies (0.3–1.4 GHz) are currently found in the range $\alpha \sim 1$ –2 (e.g. Venturi 2011). The Coma radio halo is a unique case with several spectral measurements covering about two orders of magnitude in frequency. Despite the scatter that is observed between the different measurements, a spectral steepening is observed at higher frequencies, suggesting a corresponding break in the spectrum of the emitting electrons (see Brunetti et al. 2013 and references therein).

We still lack a comprehensive understanding of the spectrum of radio haloes predicted in reacceleration models. In the context of our model and in the other turbulent reacceleration models, the spectrum of radio haloes results from the interplay between the CRE spectrum and the probability distribution function (PDF) of magnetic field strengths in the emitting volume. Simple homogeneous reacceleration models, where both the magnetic field and acceleration rate are constant in the emitting volume, predict a curved spectrum due to the interplay between energy losses and diffusion in the particle’s momentum space (e.g. Cassano & Brunetti 2005). More realistic turbulent models account (at least) for the decline of the magnetic field strength with radius in clusters. The effect is a stretching in frequency of the volume-integrated synchrotron spectrum of the haloes that allows us to successfully explain observed spectra (BL07; Brunetti et al. 2008; Brunetti & Lazarian 2011a; Donnert et al. 2013; Macario et al. 2013). In the real case of a turbulent ICM the magnetic PDF is expected to be broad, and the turbulent and plasma-collisional properties can vary in the emitting, Mpc, volume. This, combined with the possibility of CRE diffusion across different turbulent regions, is expected to stretch considerably the synchrotron spectrum in frequency. Examples of synchrotron spectra from non-homogeneous turbulent reacceleration can be found in ZuHone et al. (2013), where turbulent acceleration with $D_{pp} \propto p^2$ and synchrotron emission from mini-haloes (cluster’s core) are calculated using high-resolution (kpc) MHD simulations combined with tracer particles to follow the dynamics and evolution of CRE.

5 DISCUSSION ON CRS REACCELERATION IN THE ICM

5.1 A comparison with reacceleration by compressive turbulence

In this section, we compare our model with stochastic reacceleration models by compressible turbulence in the ICM.

We start from the momentum-diffusion coefficient that is expected in the classical *Fermi* theory. This is (e.g. Longair 2011)

$$D_{pp} \sim p^2 \frac{\delta V_l^2}{cl} \sim p^2 \frac{V_{ph}^2 (\delta B)_l^2}{cl B_0^2}, \quad (17)$$

where l is the minimum scale of eddies, V_{ph} is the phase velocity of waves and in high-beta plasma conditions it is $\delta B/B_0 \sim \delta V/V_{ph}$. It follows that D_{pp}/p^2 is simply $c/\delta V_l$ times the turn-over time of turbulent eddies at the dissipation scale.

These dependences basically apply also to the case of the interaction between compressible turbulence (essentially fast modes) and particles via TTD. TTD interacts through the $n = 0$ Landau resonance (e.g. Fisk 1976; Schlickeiser & Miller 1998). This interaction is essentially the coupling between the magnetic moment of

particles and the parallel magnetic field gradients and it uses the turbulent energy that is available on a broad range of scales, in principle between the dissipation and the injection scales. The diffusion coefficient in the particles momentum space due to TTD in the ICM is derived in BL07:

$$D_{pp} = \frac{\pi^2}{2c} \frac{p^2 c_s^2}{B_0^2} \int_{c_s/c}^1 d\mu \frac{1-\mu^2}{\mu} \left(1 - \left(\frac{c_s}{c\mu}\right)^2\right)^2 \times \int_{k_0}^{k_{cut}} dk W_B(k) k. \quad (18)$$

Similarly to the classical second-order *Fermi* mechanism, the acceleration depends on the minimum/dissipation scale of the electromagnetic fluctuations and on the energy density of these fluctuations, being $\int dk W_B k \sim k_{cut} \delta B_{k_{cut}}^2 / 8\pi$.

The dissipation scale is set by the competition between turbulent cascade and collisionless damping. Two situations are considered in the literature.

(i) The collision frequency of thermal particles is $\omega_{ii} < \omega = kc_s$. In this case, the damping of the waves is dominated by TTD with thermal particles (electrons) and $k_{cut} \sim 10^4 k_0 M_t^4$ (BL07; Miniati 2015; Brunetti 2016). We stress that under these conditions *most* of the turbulent energy is dissipated into the heating of the thermal ICM (see BL07). Assuming a Kraichnan spectrum, this leads to a reacceleration time for CRE:

$$\tau_{acc} = \frac{p^2}{4D_{pp}} \simeq 125 \left(\frac{M_t}{1/2}\right)^{-4} \left(\frac{L_0/300 \text{ kpc}}{c_s/1500 \text{ km s}^{-1}}\right). \quad (\text{Myr}) \quad (19)$$

(ii) The collisions between thermal particles in the ICM are fast, $\omega_{ii} > \omega = kc_s$. This is the case where scatterings are mediated by magnetic field perturbations driven by plasma instabilities (e.g. Lazarian & Beresnyak 2006; Brunetti & Lazarian 2011b, Santos-Lima et al. 2014, and references therein). Contrary to case (i), here the damping of the waves is due to TTD with relativistic particles (CR protons and CRE), turbulence reaches smaller scales and the reacceleration time (for Kraichnan spectrum) is (Brunetti & Lazarian 2011b)

$$\tau_{acc} \simeq 6 \left(\frac{M_t}{1/2}\right)^{-4} \left(\frac{L_0/300 \text{ kpc}}{c_s/1500 \text{ km s}^{-1}}\right) \left(\frac{\mathcal{R}_{CR}}{25}\right), \quad (\text{Myr}) \quad (20)$$

where

$$\mathcal{R}_{CR} = \sum_{i=e,p} \frac{c \int p^4 dp \frac{\partial f_i(p)}{\partial p}}{\rho_{ICM} c_s^2} \quad (21)$$

ρ_{ICM} is the thermal density of the ICM, and $f_i(p)$ is the distribution function of CRs (CRE and CR protons) in the momentum space.

The two acceleration schemes have been used extensively to explain radio haloes and mini radio haloes in galaxy clusters (BL07; Brunetti & Lazarian 2011a,b; Beresnyak et al. 2013; Donnert et al. 2013; ZuHone et al. 2013; Donnert & Brunetti 2014; Miniati 2015; Pinzke et al. 2015). The main assumptions in these studies is that compressible turbulence is a relevant part of turbulence in the ICM. Challenges of these models due to our poor understanding of the ICM microphysics have been extensively discussed in Brunetti (2016). In particular, it has been shown that an increasingly steeper spectrum of the electromagnetic fluctuations induces a slower acceleration rate essentially because fluctuations are dissipated at larger scales. Recent cosmological simulations suggest that compressive turbulence in the ICM is Burgers-like ($W \propto k^{-2}$). In this case (assuming that velocities and electromagnetic fluctuations follow the same scalings), for typical velocities of the turbulent eddies

$\delta V \sim 500\text{--}800 \text{ km s}^{-1}$ on large scales ($L_0 = 300 \text{ kpc}$), the efficiency of TTD acceleration drops by about 10 times with respect to that predicted adopting a Kraichnan spectrum (Brunetti 2016, their fig. 1). Under these unfavourable conditions in the collisionless scenario (case i, equation 19) TTD would become inefficient and would not provide a valuable scenario for the origin of cluster-scale radio emission. In this case explaining radio haloes would require that the ICM behaves mostly collisional (i.e. case ii, equation 20; see Miniati 2015).

As already mentioned, the main motivation for this paper is that large-scale turbulence in the ICM is mainly solenoidal (Miniati 2014). This incompressible turbulence is dissipated into the thermal ICM at a much smaller rate than the compressible part and consequently it provides a previously unexplored, natural energy reservoir for stochastic particle acceleration in the ICM. In this paper, we essentially suggest that part of this energy drains into relativistic particles via the interaction with magnetic field lines diffusing in turbulent reconnection. Note that the acceleration mechanism explained in Section 3.2 do not drain turbulent energy into thermal ICM as these particles do not diffuse on sufficiently large scales. Our mechanism also differs from other models for diffuse radio emission from galaxy clusters that are based on particles–waves interaction via gyro-resonance, where the non-linear coupling between particles and Alfvén waves at very small, resonant, scales $k \sim eBE^{-1}/(\mu \pm V_A/c)$ is used (Ohno, Takizawa & Shibata 2002; Fujita et al. 2003; Brunetti et al. 2004; Fujita et al. 2015). In fact, it is unlikely that gyro-resonant acceleration is driven directly by the cascade of incompressible turbulence from large scales to very small scales because the scale-dependent anisotropies that are developed in the Alfvénic cascade at MHD scales quench the acceleration (Chandran 2000; Yan & Lazarian 2004).

In our model, the acceleration drains energy essentially from the Alfvénic motions at the Alfvén scale, l_A . In principle this energy reservoir is large and of the order of the energy flux associated with the turbulence at larger scales, $V_A^3/l_A \sim \delta V^3/L_0$ for Kolmogorov spectrum. As a reference, by considering $\psi \sim 0.2\text{--}0.5$ and typical conditions for the solenoidal turbulence in the ICM, $M_t^2 \sim 0.3\text{--}0.8$ and $L_0 = 100\text{--}500 \text{ kpc}$ (consistent with numerical simulations), the acceleration rates (Section 4.2) are similar to those expected in the case of collisionless TTD with compressive turbulence for Kraichnan spectrum (case i, equation 19).⁴ Since collisionless TTD has been successfully applied to radio haloes, we conclude that our mechanism may provide a valuable alternative to the mechanisms based on compressible turbulence or that it may play a role in combination with these other mechanisms.

5.2 Dampings and saturation effects

TTD reacceleration by compressible turbulence in the ICM has been calculated considering self-consistently acceleration and turbulent-damping rates (BL07; Brunetti & Lazarian 2011a, Brunetti & Lazarian 2011b). On the other hand, in Section 3 we have calculated the diffusion coefficient in the particles’ momentum space in the test particle regime. If a large fraction of the turbulent energy flux in our model is channelled into CRs, saturation effects become

⁴ This is also equivalent to acceleration rates expected in the case of collisional TTD (ii, equation 20) assuming Burgers-like spectrum of turbulence, or in the case of Kraichnan spectrum assuming smaller values of the turbulent Mach number, $M_t^2 \sim 0.05\text{--}0.1$.

important. Acceleration and turbulent damping, Γ , are connected through detailed balancing:

$$\sum_{i=e,p} \int d^3 p E \frac{\partial f_i}{\partial t} = \int d^3 k W(\mathbf{k}) \Gamma(\mathbf{k}), \quad (22)$$

where the left-hand side of equation (22) accounts for the energy channelled into CRs and the right-hand side accounts for the energy that is extracted from turbulence via damping; $W(\mathbf{k})$ is the 3D turbulent spectrum ($W(\mathbf{k}) = 4\pi k^2 W(k)$ in the isotropic case). Assuming pitch-angle isotropy of CRs, the time-evolution of the CRs momentum distribution in equation (22) depends on the momentum-diffusion coefficient via

$$\frac{\partial f_i}{\partial t} = \frac{1}{p^2} \frac{\partial}{\partial p} \left(p^2 D_{pp} \frac{\partial f}{\partial p} \right) \quad (23)$$

and the evolution of the turbulent spectrum is given by (see e.g. BL07 and references therein)

$$\frac{\partial W}{\partial t} = \frac{\partial}{\partial k} \left(k^2 D_{kk} \frac{\partial}{\partial k} \left(\frac{W(k)}{k^2} \right) \right) - \Gamma W(k) + I(k), \quad (24)$$

where the first and second terms in the right-hand side account for turbulent cascade and damping, respectively, $D_{kk} \sim k^2/\tau_{kk}$ is the diffusion coefficient in the wavenumber space,⁵ τ_{kk} is the turbulent cascading-time at scale k^{-1} , and $I(k)$ accounts for the process of injection of turbulence at large scales.

Equations (22)–(24) connect acceleration rate, CR energy densities and turbulent damping and cascading. They essentially imply that the increase of the energy density of CRs with time produces a stronger damping, with the consequence that the turbulent spectrum is gradually suppressed and that acceleration is reduced. In this regime, full Fokker–Planck time-dependent calculations, combined with the modelling of the evolution of the turbulent spectrum, are necessary for a correct evaluation of the acceleration process (see e.g. Brunetti et al. 2004; Brunetti & Lazarian 2011b for examples of calculations in the ICM). These saturation effects also limit the applicability of the approach used in Section 4.2, that is based on the scaling of the (spectral) analysis in compressive turbulent acceleration to the case of (incompressible) turbulent reconnection.

In our acceleration model, the turbulent eddies on scale $\sim l_A$ are the most important ones. Consequently, the importance of saturation effects can be evaluated by comparing damping and turbulent cascade at these scales: if damping rate is smaller than the rate of turbulent cascade, $\tau_{l_A l_A}^{-1} \sim V_A l_A^{-1}$, the turbulent spectrum is not modified and saturation effects are not important. This is the case when the energy flux of turbulent cascade at the Alfvén scale, $\sim \rho_{\text{ICM}} V_A^3 l_A^{-1}$, is much larger than the energy flux that is channelled into CRs. The two quantities can be connected via

$$\rho_{\text{ICM}} V_A^3 l_A^{-1} \eta_{\text{CR}} \sim c \int d^3 p \frac{1}{p} \frac{\partial}{\partial p} \left(p^2 D_{pp} \frac{\partial f}{\partial p} \right), \quad (25)$$

where η_{CR} is the fraction of turbulent energy flux that is transferred into CRs by our mechanism, and D_{pp} is given in equation (8). The limit $\eta_{\text{CR}} \rightarrow 1$ corresponds to strong damping. In fact, this limit constrains the minimum value of ψ that is allowed in test-particle calculations (i.e. neglecting saturation/damping effects) of our model. From equations (8) and (25) this is

$$\psi_{\text{min}} \sim \left(\frac{5}{2} \beta_{\text{pl}} \frac{V_A}{c} \frac{\epsilon_{\text{CR}} \mathcal{S}_{\text{CR}}}{\rho_{\text{ICM}} c_s^2} \right)^{1/3}, \quad (26)$$

⁵ More specifically it is $\tau_{kk} = k^3 / \frac{\partial}{\partial k} (D_{kk} k^2)$.

where we define

$$\mathcal{S}_{\text{CR}} = \frac{\sum_{i=e,p} \int d^3 p \frac{1}{p} \frac{\partial}{\partial p} \left(p^4 \frac{\partial f_i}{\partial p} \right)}{\sum_{i=e,p} \int d^3 p f_i(p) p}. \quad (27)$$

As expected, limits on ψ depend on the energy density of CRs in the ICM. Theoretical reasons suggest that CR protons are the most important CR component in galaxy clusters (see BJ14 for review). In the recent years, γ -ray and radio observations allowed us to constrain the energy density that is associated with CR protons in the central Mpc-regions of galaxy clusters, $\epsilon_{\text{CR}} < \text{few } 0.01 \times \epsilon_{\text{ICM}}$ (see e.g. Brunetti et al. 2007, Brunetti et al. 2008; Ackermann et al. 2010, 2014; Zandanel & Ando 2014; BJ14 for review). If we use these reference values, equation (26) basically implies $\psi > 0.1$.⁶ This limit on ψ is fully consistent with the values used/derived in Section 4.2 to explain cluster-scale radio emission.

Interestingly for $\psi \sim 0.1$, the turbulent velocities that are necessary to explain radio haloes are still significant $\delta V_o > 100 \text{ km s}^{-1}$ [for example >90 and $>160(L_o/100)^{1/3}(n_{\text{ICM}}/10^{-3})^{-1/6} \text{ km s}^{-1}$ for the radio haloes in Coma and Bullet clusters, respectively, see Section 4]. This essentially sets the level of the minimum turbulent broadening of the profile of X-ray lines that is expected in our model. Non-detection of such a broadening with future X-ray spectrometers, for example with ATHENA, will rule out our model under the conditions explored in this paper (namely fast diffusion approximation and $\Delta p \ll p$, Section 3.2).⁷

5.3 Reacceleration of CR protons

As a final remark, we point out that in principle our mechanism reaccelerate also CR protons that will accumulate their energy more efficiently than CRe (because CRp are subject to less efficient energy losses; see BJ14 for a review). The energy density accumulated by CR protons in a reacceleration time Δt will be

$$\rho_{\text{ICM}} V_A^3 l_A^{-1} \langle \eta_{\text{CR}} \rangle_{\Delta t} \Delta t \approx \Delta t \int d^3 p E \frac{\partial f_p}{\partial t} \sim \delta \epsilon_{\text{CR}}, \quad (28)$$

where $\langle \eta_{\text{CR}} \rangle_{\Delta t} \Delta t = \int_0^{\Delta t} \eta_{\text{CR}}(t) dt$.

In practice, CR protons will release part of this energy due to losses in Gyr-time-scales. In a few Gyr, CR protons will be also advected and transported by large-scale motions on scales larger than the relevant turbulent scales and thus energy will be redistributed on large-scales decreasing $\delta \epsilon_{\text{CR}}$. Nevertheless, we can use equation (28) under the condition $\delta \epsilon_{\text{CR}} < \epsilon_{\text{CR}}$ to derive a (order of magnitude) limit on Δt ; it is useful also to check if our calculations in the case of radio haloes are self-consistent. This is (from equations 25, 8 and 28)

$$\Delta t \sim \frac{c}{3} \frac{l_A}{V_A^2} \frac{\epsilon_{\text{CR}}(\delta \epsilon_{\text{CR}}/\epsilon_{\text{CR}})}{\langle \epsilon_{\text{CR}}(t) \mathcal{S} \rangle_{\Delta t}} \psi^3, \quad (29)$$

where $l_A = M_l^{-3} L_o (V_A/c_s)^3$. At this point, equation (29) can be combined with the Mach number that is required to generate radio haloes with observed synchrotron steepening frequency ν_o (under the minimal condition $B \sim B_{\text{cmb}}/\sqrt{3}$, equation 16):

$$\Delta t \sim \left(\frac{\nu_o(\text{GHz})}{3} \frac{7}{\xi} \right)^{-1/2} (1+z)^{-7/2} \frac{\epsilon_{\text{CR}}(\delta \epsilon_{\text{CR}}/\epsilon_{\text{CR}})}{\langle \epsilon_{\text{CR}}(t) \mathcal{S} \rangle_{\Delta t}}, \quad (\text{Gyr}) \quad (30)$$

⁶ On the other hand, if we consider only CRe in the ICM, or an ad hoc situation where CR protons are not accelerated by our mechanism, it is $\mathcal{S}_{\text{CRe}} \epsilon_{\text{CRe}} \sim 10^{-5} - 10^{-4} \rho_{\text{ICM}} c_s^2$ and essentially $\psi > 0.02$.

⁷ Alternatively, it will require an ad hoc situation where CRp are not accelerated efficiently by our mechanism.

where typically $\epsilon_{\text{CR}}/\langle \epsilon_{\text{CR}}(t) \mathcal{S} \rangle_{\Delta t} \gtrsim 1$. We thus conclude that radio haloes observed at GHz frequencies can be generated by our mechanism for Gyr. These time-scales are comparable to the lifetimes of radio haloes evaluated from statistical analysis (e.g. Brunetti et al. 2009; BJ14) suggesting that the exploratory (test-particle) calculations in Sections 3.2 and 4 provide a good approximation. A reliable modelling of the acceleration process for longer acceleration periods (or for radio haloes with spectra extending to $\nu_o \gg \text{few GHz}$) requires full Fokker–Planck time-dependent calculations combined with numerical simulations of clusters (including CRs transport).

6 SUMMARY

We suggest that relativistic particles diffusing in super-Alfvénic incompressible turbulence gain energy due to the statistical interaction with field lines in regions of magnetic reconnection and turbulent dynamo. In view of large-scale turbulence being present in the ICM, we assume a scheme based on turbulent reconnection and assume that MHD turbulence provides a good guide as far as reconnection is considered. We calculate the acceleration rate in the fast diffusion regime and in the limit $\Delta p \ll p$. Under these conditions, the mechanism is essentially a second-order *Fermi*.

In this exploratory paper, we account for the interaction between magnetic field lines and CRe on large scales, ~ 0.1 – 1 kpc, assuming transport properties and turbulent scalings that follow from MHD turbulence. Additional kinetic effects on smaller scales may affect the physics of reconnection and CRe transport and acceleration. For this reason, we consider CRe mfp as a free parameter that is however bounded by the combination of basic constraints, including the confinement of CRe (Section 3.2), the interaction with large-scale fields (Section 3.2) and indirect considerations on the turbulent energy flux that is available (Section 5).

We propose that the mechanism may play a role for the origin of radio haloes and large-scale diffuse emission in galaxy clusters. In fact, assuming reliable conditions in the ICM we have shown that the expected reacceleration rate is similar to that of classical reacceleration models proposed for radio haloes, provided that the CRe mfp is a fraction ~ 0.1 – 0.5 of the MHD scale. Smaller values of the mfp would make the mechanism even more efficient, however in this case saturation/damping effects (Section 5.2) should become important invalidating the test-particle approach adopted in our paper and deserve future studies.

Similarly to previous reacceleration models, the diffusion coefficient in the momentum space is $D_{pp} \propto p^2$ and thus, in principle all previous results based on solutions of Fokker–Planck equations can be easily extended to our case. However our approach differs from these previous models because it is based on the incompressible part of the turbulence and because it is mediated by turbulent reconnection and dynamo. According to current numerical cosmological simulations, incompressible turbulence in the ICM is found to be dominant, super-Alfvénic and *quasi*-sonic and thus the new mechanism explored in our paper appears particularly appealing. Interestingly, in our mechanism the conditions that are necessary to generate radio haloes have unavoidable consequences on the broadening of the profile of X-ray lines, allowing a test of model assumptions with forthcoming X-ray calorimeters (ASTRO-H, ATHENA).

This is an exploratory paper.

One of the critical points is the particles mfp. The combined effect of super-Alfvénic motions and resonant mirroring with pseudo-Alfvén modes constrains the mfp \sim a fraction of the MHD scale. However in a more general situation, additional scattering agents

induced by additional turbulent components may reduce the mfp; this might have the potential to increase the acceleration rate.

Another critical point is the assumption of turbulent reconnection scheme. The basic assumption here is that reconnection is part of the MHD cascade. This appears quite natural in the ICM given the presence of large-scale turbulence that can be driven at large scales in merging clusters and given the observed connection between mergers and non-thermal emission from galaxy clusters. Other schemes, such as tearing reconnection, do not invalidate *per se* our reacceleration scheme, provided that reconnection and dynamo are still triggered by large-scale motions. This however requires an extension of our modelling.

Calculations in this paper focus on the hypothesis of fast-diffusion regime and $\Delta p \ll p$ (Section 3.2). Numerical simulations can be used to extend this exploratory study to the situation $\Delta p \sim p$, in which case the mechanism is expected to differ significantly from a second-order *Fermi*. Simulations will also allow us to calculate the acceleration rate under more realistic configurations of reconnection and dynamo regions.

Finally, it is worth to mention that in our model we focus on the reacceleration of CRE. Also CR protons, if present, will be reaccelerated by our mechanism. As a sanity-check, we have shown that, assuming the physical parameters that are required to explain radio haloes, the energy budget of CR protons resulting from a reacceleration period comparable to the lifetime of haloes is consistent with current limits from γ -ray observations. At this point, since reacceleration rates and diffusion coefficient, $D_{pp} \propto p^2$, in our model are equivalent/similar to those in lepto-hadronic reacceleration models where CR protons and their secondary particles have been explicitly taken into account (e.g. Brunetti & Lazarian 2011a, Brunetti et al. 2012; Pinzke et al. 2015), also the conclusions of these previous works can be extended to our picture.

ACKNOWLEDGEMENTS

We thank the referee for useful comments that have improved the presentation of the paper. GB and AL acknowledge support from the Alexander von Humboldt Foundation and discussions with professor R. Schlickeiser. GB acknowledges support from PRIN-INAF 2014, AL acknowledges support from NASA grant NNX14AJ53G.

REFERENCES

Ackermann M. et al., 2010, *ApJ*, 717, L71
 Ackermann M. et al., 2014, *ApJ*, 787, 18
 Beresnyak A., 2013, preprint (arXiv:1301.7424)
 Beresnyak A., Lazarian A., 2015, in Lazarian A., de Gouveia Dal Pino E. M., Melioli C., eds, *Astrophysics and Space Science Library*, Vol. 407, *Magnetic Fields in Diffuse Media*. Springer, Berlin, p. 163
 Beresnyak A., Yan H., Lazarian A., 2011, *ApJ*, 728, 60
 Beresnyak A., Xu H., Li H., Schlickeiser R., 2013, *ApJ*, 771, 131
 Bhattacharjee A., 2004, *ARA&A*, 42, 365
 Birn J. et al., 2001, *J. Geophys. Res.*, 106, 3715
 Brügggen M., Vazza F., 2015, in Lazarian A., de Gouveia Dal Pino E. M., Melioli C., eds, *Astrophysics and Space Science Library*, Vol. 407, *Magnetic Fields in Diffuse Media*. Springer, Berlin, p. 599
 Brunetti G., 2016, *Plasma Phys. Control. Fusion*, 58, 014011
 Brunetti G., Jones T. W., 2014, *Int. J. Mod. Phys. D*, 23, 1430007 (BJ14)
 Brunetti G., Lazarian A., 2007, *MNRAS*, 378, 245 (BL07)
 Brunetti G., Lazarian A., 2011a, *MNRAS*, 410, 127
 Brunetti G., Lazarian A., 2011b, *MNRAS*, 412, 817
 Brunetti G., Setti G., Ferretti L., Giovannini G., 2001, *MNRAS*, 320, 365
 Brunetti G., Blasi P., Cassano R., Gabici S., 2004, *MNRAS*, 350, 1174

Brunetti G., Venturi T., Dallacasa D., Cassano R., Dolag K., Giacintucci S., Setti G., 2007, *ApJ*, 670, L5
 Brunetti G., Cassano R., Dolag K., Setti G., 2009, *A&A*, 507, 661
 Brunetti G., Blasi P., Reimer O., Rudnick L., Bonafede A., Brown S., 2012, *MNRAS*, 426, 956
 Brunetti G., Rudnick L., Cassano R., Mazzotta P., Donnert J., Dolag K., 2013, *A&A*, 558, A52
 Brunetti G. et al., 2008, *Nature*, 455, 944
 Carilli C. L., Taylor G. B., 2002, *ARA&A*, 40, 319
 Cassano R., Brunetti G., 2005, *MNRAS*, 357, 1313
 Cassano R., Brunetti G., Röttgering H. J. A., Brügggen M., 2010, *A&A*, 509, A68
 Cassano R. et al., 2013, *ApJ*, 777, 141
 Chandran B. D. G., 2000, *Phys. Rev. Lett.*, 85, 4656
 Cuciti V., Cassano R., Brunetti G., Dallacasa D., Kale. R., Etori S., Venturi T., 2015, *A&A*, 580, A97
 Daughton W., Roytershteyn V., Karimabadi H., Yin L., Albright B. J., Bergen B., Bowers K. J., 2011, *Nat. Phys.*, 7, 539
 de Gouveia dal Pino E. M., Lazarian A., 2005, *A&A*, 441, 845
 Donnert J., Brunetti G., 2014, *MNRAS*, 443, 3564
 Donnert J., Dolag K., Brunetti G., Cassano R., 2013, *MNRAS*, 429, 3564
 Drake J. F., Swisdak M., Che H., Shay M. A., 2006, *Nature*, 443, 553
 Drake J. F., Opher M., Swisdak M., Chamoun J. N., 2010, *ApJ*, 709, 963
 Drake J. F., Swisdak M., Fermo R., 2013, *ApJ*, 763, L5
 Drury L. O' C., 2012, *MNRAS*, 422, 2474
 Etori S. et al., 2013, preprint (arXiv:1306.2322)
 Eyink G. L., Lazarian A., Vishniac E. T., 2011, *ApJ*, 743, 51
 Eyink G. L., 2015, *ApJ*, 807, 137
 Eyink G. et al., 2013, *Nature*, 497, 466
 Feretti L., Giovannini G., Govoni F., Murgia M., 2012, *A&AR*, 20, 54
 Fisk L. A., 1976, *J. Geophys. Res.*, 81, 4633
 Fujita Y., Takizawa M., Sarazin C. L., 2003, *ApJ*, 584, 190
 Fujita Y., Takizawa M., Yamazaki R., Akamatsu H., Ohno H., 2015, *ApJ*, 815, 116
 Giannios D., 2013, *MNRAS*, 431, 355
 Kadowaki L. H. S., de Gouveia Dal Pino E. M., Singh C. B., 2015, *ApJ*, 802, 113
 Karimabadi H., Lazarian A., 2013, *Phys. Plasmas*, 20, 112102
 Khiali B., de Gouveia Dal Pino E. M., del Valle M. V., 2015, *MNRAS*, 449, 34
 Kitayama T. et al., 2014, preprint (arXiv:1412.1176)
 Kowal G., Lazarian A., Vishniac E. T., Otmianowska-Mazur K., 2009, *ApJ*, 700, 63
 Kowal G., de Gouveia Dal Pino E. M., Lazarian A., 2011, *ApJ*, 735, 102
 Kowal G., de Gouveia Dal Pino E. M., Lazarian A., 2012, *Phys. Rev. Lett.*, 108, 241102
 Lalescu C. C., Shi Y.-K., Eyink G. L., Drivas T. D., Vishniac E. T., Lazarian A., 2015, *Phys. Rev. Lett.*, 115, 025001
 Lazarian A., Beresnyak A., 2006, *MNRAS*, 373, 1195
 Lazarian A., Brunetti G., 2011, *Mem. Soc. Astron. Ital.*, 82, 636
 Lazarian A., Desiati P., 2010, *ApJ*, 722, 188
 Lazarian A., Opher M., 2009, *ApJ*, 703, 8
 Lazarian A., Vishniac E. T., 1999, *ApJ*, 517, 700 (LV99)
 Lazarian A., Eyink G. L., Vishniac E. T., Kowal G., 2015, in Lazarian A., de Gouveia Dal Pino E. M., Melioli C., eds, *Astrophysics and Space Science Library*, Vol. 407, *Magnetic Fields in Diffuse Media*. Springer, Berlin, p. 311
 Le Roux J. A., Zank G. P., Webb G. M., Khabarova O., 2015, *ApJ*, 801, 112
 Liang H., Hunstead R. W., Birkinshaw M., Andreani P., 2000, *ApJ*, 544, 686
 Longair M. S., 2011, *High Energy Astrophysics*. Cambridge Univ. Press, Cambridge
 Loureiro N. F., Schekochihin A. A., Cowley S. C., 2007, *Phys. Plasmas*, 14, 100703
 Lyubarsky Y. E., 2003, *MNRAS*, 345, 153
 Lyutikov M., Blandford R., 2003, preprint (astro-ph/0312347)
 Macario G. et al., 2013, *A&A*, 551, A141
 Makwana K. D., Zhdankin V., Li H., Daughton W., Cattaneo F., 2015, *Phys. Plasmas*, 22, 042902

- Marchegiani P., Colafrancesco S., 2015, *MNRAS*, 452, 1328
- Mertsch P., 2011, *J. Cosmol. Astropart. Phys.*, 12, 010
- Miniati F., 2014, *ApJ*, 782, 21
- Miniati F., 2015, *ApJ*, 800, 60
- Miniati F., Beresnyak A., 2015, *Nature*, 523, 59
- Ng J., Huang Y.-M., Hakim A., Bhattacharjee A., Stanier A., Daughton W., Wang L., Germaschewski K., 2015, *Phys. Plasmas*
- Ohno H., Takizawa M., Shibata S., 2002, *ApJ*, 577, 658
- Oishi J. S., Mac Low M.-M., Collins D. C., Tamura M., 2015, *ApJ*, 806, L12
- Owen F. N., Rudnick L., Eilek J., Rau U., Bhatnagar S., Kogan L., 2014, *ApJ*, 794, 24
- Parker E. N., 1957, *J. Geophys. Res.*, 62, 509
- Petrosian V., 2001, *ApJ*, 557, 560
- Petrosian V., East W. E., 2008, *ApJ*, 682, 175
- Petschek H. E., 1964, *NASA Special Publication*, 50, 425
- Pinzke A., Oh S. P., Pfrommer C., 2015, preprint ([arXiv:1503.07870](https://arxiv.org/abs/1503.07870))
- Porter D. H., Jones T. W., Ryu D., 2015, *ApJ*, 810, 93
- Ryu D., Kang H., Cho J., Das S., 2008, *Science*, 320, 909
- Santos-Lima R., de Gouveia Dal Pino E. M., Kowal G., Falceta-Goncalves D., Lazarian A., Nakwacki M. S., 2014, *ApJ*, 781, 84
- Schlickeiser R., 1984, *A&A*, 136, 227
- Schlickeiser R., 2002, *Astronomy and Astrophysics Library, Cosmic Ray Astrophysics*. Springer, Berlin
- Schlickeiser R., Miller J. A., 1998, *ApJ*, 492, 352
- Shay M. A., Drake J. F., Denton R. E., Biskamp D., 1998, *J. Geophys. Res.*, 103, 9165
- Shimwell T. W., Brown S., Feain I. J., Feretti L., Gaensler B. M., Lage C., 2014, *MNRAS*, 440, 2901
- Sironi L., Spitkovsky A., 2014, *ApJ*, 783, L21
- Sweet P. A., 1958, in Lehnert B., ed., *Proc. IAU Symp. 6, Electromagnetic Phenomena in Cosmical Physics*. Cambridge Univ. Press, Cambridge, p. 123
- Uzdensky D. A., Loureiro N. F., Schekochihin A. A., 2010, *Phys. Rev. Lett.*, 105, 235002
- Vazza F., Brunetti G., Gheller C., Brunino C., Brüggén M., 2011, *A&A*, 529, A17
- Venturi T., 2011, *Mem. Soc. Astron. Ital.*, 82, 499
- Yan H., Lazarian A., 2004, *ApJ*, 614, 757
- Yan H., Lazarian A., 2008, *ApJ*, 673, 942
- Zandanel F., Ando S., 2014, *MNRAS*, 440, 663
- Zank G. P., Le Roux J. A., Webb G. M., Dosch A., Khabarova O., 2014, *ApJ*, 797, 28
- Zhang B., Yan H., 2011, *ApJ*, 726, 90
- ZuHone J. A., Markevitch M., Brunetti G., Giacintucci S., 2013, *ApJ*, 762, 78

This paper has been typeset from a $\text{\TeX}/\text{\LaTeX}$ file prepared by the author.